RESEARCH ARTICLE | JULY 19 2023

8.1 μ m-emitting InP-based quantum cascade laser grown on Si by metalorganic chemical vapor deposition Θ

S. Xu ⊚ ; S. Zhang ⊚ ; J. D. Kirch ⊚ ; H. Gao; Y. Wang ⊚ ; M. L. Lee ⊚ ; S. R. Tatavarti ⊚ ; D. Botez ⊚ ; L. J. Mawst ᢦ ⊚



Appl. Phys. Lett. 123, 031110 (2023) https://doi.org/10.1063/5.0155202

A CHORUS





CrossMark

500 kHz or 8.5 GHz? And all the ranges in between.

Lock-in Amplifiers for your periodic signal measurement









8.1 μ m-emitting InP-based quantum cascade laser grown on Si by metalorganic chemical vapor deposition

Cite as: Appl. Phys. Lett. **123**, 031110 (2023); doi: 10.1063/5.0155202 Submitted: 18 April 2023 · Accepted: 6 July 2023 · Published Online: 19 July 2023







S. Xu, D. S. Zhang, D. J. D. Kirch, D. H. Gao, Y. Wang, D. M. L. Lee, D. S. R. Tatavarti, D. Botez, D. Bot

AFFILIATIONS

- ¹Department of Electrical and Computer Engineering, University of Wisconsin, Madison, Wisconsin 53706, USA
- ²Holonyak Micro & Nanotechnology Laboratory, University of Illinois Urbana-Champaign, Urbana, Illinois 61801, USA

ABSTRACT

This study presents the growth and characterization of an 8.1 μ m-emitting, InGaAs/AlInAs/InP-based quantum cascade laser (QCL) formed on an InP-on-Si composite template by metalorganic chemical vapor deposition (MOCVD). First, for the composite-template formation, a GaAs buffer layer was grown by solid-source molecular-beam epitaxy on a commercial (001) GaP/Si substrate, thus forming a GaAs/GaP/Si template. Next, an InP metamorphic buffer layer (MBL) structure was grown atop the GaAs/GaP/Si template by MOCVD, followed by the MOCVD growth of the full QCL structure. The top-surface morphology of the GaAs/GaP/Si template before and after the InP MBL growth was assessed via atomic force microscopy, over a $100~\mu\text{m}^2$ area, and no antiphase domains were found. The average threading dislocation density (TDD) for the GaAs/GaP/Si template was found to be $\sim 1 \times 10^9 \, \text{cm}^{-2}$, with a slightly lower defect density of $\sim 7.9 \times 10^8 \, \text{cm}^{-2}$ after the InP MBL growth. The lasing performance of the QCL structure grown on Si was compared to that of its counterpart grown on InP native substrate and found to be quite similar. That is, the threshold-current density of the QCL on Si, for deep-etched ridge-guide devices with uncoated facets, is somewhat lower than that for its counterpart on native InP substrate, 1.50 vs 1.92 kA/cm², while the maximum output power per facet is 1.64 vs 1.47 W. These results further demonstrate the resilience of QCLs to relatively high residual TDD values.

Published under an exclusive license by AIP Publishing. https://doi.org/10.1063/5.0155202

The integration of high-performance optoelectronic devices as active optoelectronic components onto silicon substrates is critical to realizing chip-scale, reliable, and mass producible photonic integrated circuits (PICs). Hybrid integration methods rely on accurate alignment for efficient waveguide-to-laser optical coupling, which, in turn, requires tight fabrication processing tolerances.² Direct integration onto Si by heteroepitaxy enables the potential for mid-infrared (IR) optoelectronics integrated with mature CMOS-compatible Si platforms at low cost and with high throughput.³ At present, InGaAs/ AlInAs quantum cascade lasers (QCLs) are the prime candidates for high-power mid-IR light sources, which are generally grown on native InP substrates. The technical challenge remaining is to overcome the defects and epitaxial growth-related issues, which arise from the large lattice-constant and thermal-expansion mismatch between native substrates, such as InP and Si (e.g., ~8% lattice mismatch and ~50% thermal-expansion coefficient mismatch).

Recently, by employing direct heteroepitaxial growth on Si, room-temperature (RT) operation from all-binary InAs-based QCLs grown on Si by molecular-beam epitaxy (MBE) for long-wavelength infrared (LWIR) emission at \sim 8 (Ref. 5) and \sim 11 μ m has been demonstrated; the work was extended to \sim 14 μ m emission from QCLs grown on Ge.⁷ That research demonstrated low threshold currents and pulsed-device performances comparable to those of QCLs grown on the native InAs substrate. Ternary InGaAs/AlInAs/InP-based QCLs on Si, also grown by MBE, have been reported with operating temperatures ranging from 170 (Ref. 8) to 358 K⁹ for 4–5 μ m emission wavelengths. Output powers exceeding 2W per facet under RT pulsed-current operation were recently reported for LWIR emission by taking advantage of reduced laser-core strain relative to InP, ^{10,11} although the threshold-current densities were higher compared to those of same devices grown on native InP substrates. The aforementioned achievements have relied on laser active-core region growth by

MicroLink Devices Inc., Niles, Illinois 60714, USA

a) Author to whom correspondence should be addressed: ljmawst@wisc.edu

MBE on miscut Si substrates. By contrast, we report on QCLs grown by metalorganic chemical vapor deposition (MOCVD) on a Si substrate with nominally exact (001) orientation, which is an approach suitable for high-throughput industrial-scale production and compatible with current CMOS technologies. There are no prior reports of QCLs grown by metalorganic chemical vapor deposition (MOCVD) on Si substrates. Previously, we have demonstrated InP-based QCLs with lattice-matched ternary active-core material grown on GaAs via full MOCVD growth, which showed even lower threshold-current density and similar output-power performance compared to their counterparts grown on native InP substrate, thus demonstrating the relative insensitivity of device-performance metrics to the high residual threading dislocation density (TDD) for intersubband-transition lasers. 12 In contrast, surface roughening from non-two-dimensional growth on defect sites leads to the gradual breakdown in the superlattice structure during the active-core growth, especially for the case of strained-layer active-core regions, which may be one factor explaining the QCLs' performance degradation observed when grown on Si.1 Therefore, a low-roughness and low-defect InP-on-Si composite template together with growth optimization for the active-core region materials are needed for realizing high-performance InP-based QCLs on Si via monolithic heteroepitaxy. For this work, we adopted an InPbuffer layer with strained dislocation filters, ¹² grown onto a GaAs/ GaP/Si template, as the transition region from GaAs to relaxed InP, which then serves as the virtual substrate for the QCL growth by MOCVD. The results show that the performance of the QCL grown on Si is comparable to that of a QCL grown on native InP substrate, in spite of the relatively high TDD values and a rougher InP-buffer

To manage the large mismatch between InP and Si, a GaAsbased structure was deposited by solid-source molecular-beam epitaxy (SS-MBE) on top of a commercially available (001) GaP/Si substrate from NAsP_{III-V} GmbH, in order to create the initial template, and then the same InP MBL on GaAs process described in Ref. 12 was employed to complete the composite template. More specifically, the GaAs-based structure was formed by SS-MBE by using the following steps. A 100 nm-thick GaAs layer was first grown at a low temperature of 500 °C, with a V/III ratio of 30. Then, the growth temperature was raised to 580°C, and a 200 nm-thick GaAs layer was deposited. A 100 nm-thick In_{0.1}Ga_{0.9}As layer was inserted as a dislocation filter, which was capped, at a growth temperature of 500 °C, with a 10 nmthick GaAs protection layer; finally, a 90 nm-thick GaAs layer was grown at higher temperature of 610 °C, with a V/III ratio of 15. The total thickness of GaAs and $In_{0.1}Ga_{0.9}As$ layers was kept at 0.5 μm in order to minimize the total III-V thickness and thermal stress, at the expense of an escalated TDD value. Next, an InP metamorphic buffer layer (MBL) was grown via MOCVD on the GaAs/GaP/Si template, with a structure of four periods of three-repetition strained ~2 nm In As and \sim 37 nm In P multi-quantum-well pairs, as dislocation filters. The MOCVD growth details of the InP MBL and lattice-matched QCL structure as well as details of the device fabrication process can be found in Ref. 12. In addition, one 2-in., n-type-doped InP wafer was placed, at the same time in the growth chamber, for direct-device comparison later. A schematic diagram of the entire QCL structure grown on InP or on Si is shown in Fig. 1, with the structural details of the InP-on-Si composite template inserted on the right. Despite the total thickness of the full QCL-on-Si structure being \sim 13 μ m, no

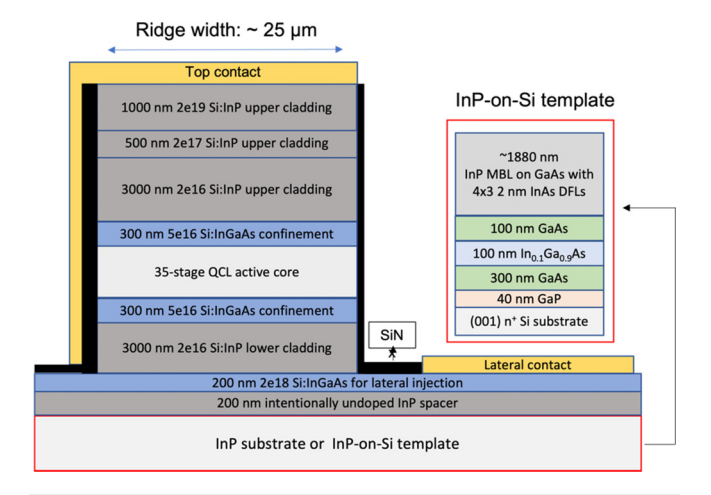


FIG. 1. Schematic representation of the full 35-stage, lattice-matched QCL structure, with 25 μm -wide ridge and lateral-current injection architecture, grown on InP substrate or on InP-on-Si composite template. The inset shows the structural details of the InP-on-Si template, which contains InAs dislocation filter layers (DFLs). The total epitaxial thickness, including metamorphic buffer layers and the laser structure, grown on Si is approximately 13 μm .

cracking was observed on the sample surface upon inspection via optical microscopy. There are two factors: the small sample size used in this study (1.7 \times 1.7 cm²) for growth on the InP-on-Si composite template, and the thick silicon substrate ($\sim\!800\,\mu\text{m}$) might help alleviate the curvature accumulation across the InP-on-Si sample.

The material surface morphology/roughness and defect density of (1) the as-grown GaAs/GaP/Si template, (2) after InP MBL growth on the template, and (3) after further growth of a 1 μ m-thick slightly strained superlattice (250-repetition of 2/2 nm In_{0.59}Ga₀.41As/ Al_{0.58}In_{0.42}As) with a InP cap layer were characterized by atomic force microscopy (AFM) and electron channeling contrast imaging (ECCI), respectively. As shown in Fig. 2(a), no antiphase domains (APD) were found on the as-grown GaAs/GaP/Si template, which has been an issue observed for III-V materials grown on Si substrates, and such surface defects could be differentiated from the top surface morphology. 14 We did not expect APDs to be present in subsequent III/V growths atop the starting template [i.e., GaP-on-Si template (NAsP_{III-V})] since it is free of APDs. The RMS roughness of the GaAs/GaP/Si template was around 1.62 nm. The template surface was smoothed after growing the InP MBL (i.e., an RMS roughness value of 1.53 nm), although still significantly rougher than for the same MBL structure grown on GaAs (i.e., \sim 0.4 nm). ¹² However, step-flow terrace features could be observed [Fig. 2(b)]. A 1- μ m thick superlattice (SL) was further grown to mimic the QCL's superlattice active-core region growth on the composite template. Then, the surface roughness was further reduced to 1.29 nm, as shown in Fig. 2(c). Figures 2(d)-2(f) show representative ECCI images of the above-mentioned samples in order to estimate the TDD value. The average TDD for the as-grown GaAs/GaP/Si template was found to be $\sim 1.0 \times 10^9 \, \text{cm}^{-2}$, with a lower density of \sim 7.9 \times 10⁸ cm⁻² after the InP MBL growth. [The line-like features in Fig. 2(d) come from misfit dislocations surrounding the In_{0.1}Ga_{0.9}As dislocation filter incorporated within the MBE-grown GaAs layer.]

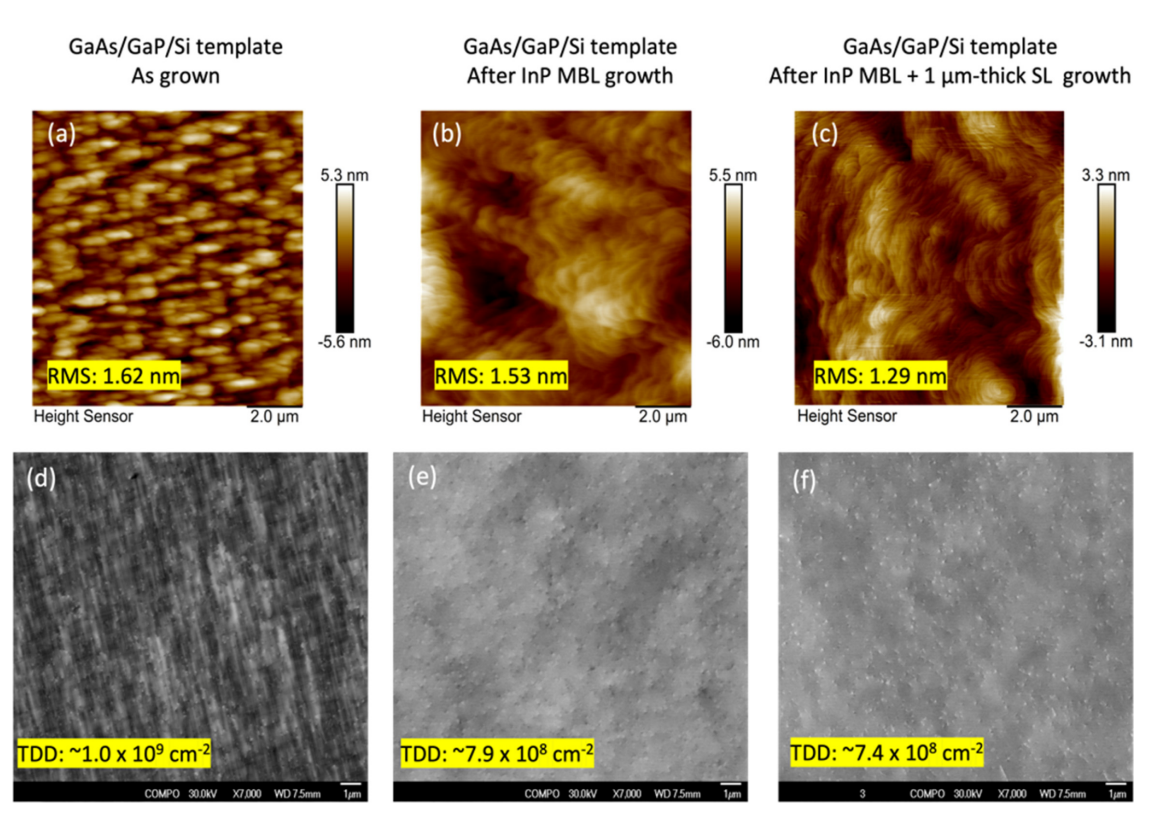


FIG. 2. Upper row: $10 \times 10 \ \mu\text{m}^2$ AFM images; lower row: ECCI images at $7000 \times$ magnification of samples. (a) and (d) MBE as-grown GaAs/GaP/Si template, (b) and (e) template after InP MBL growth, and (c) and (f) template with InP MBL after 1 μ m-thick superlattice growth.

A similar TDD value was observed after growing the 1 μ m-thick SL. Clear reflection interference fringes and only a slight intensity reduction in the last \sim 50 repetitions of the SL growth were observed by *in situ* reflectance measurement. Therefore, only minor material degradation occurs after growing the InP MBL and \sim 1 μ m-thick 250-repetition SL, and as such, the same growth conditions were applied when growing the full lattice-matched QCL structure on Si.

Overall, the trends observed from surface roughness via AFM and estimated defect density via ECCI are consistent with the relatively large full-width at half-maximum (FWHM) values measured from high-resolution x-ray resolution diffraction (HR-XRD) (004) ω -2 θ scans: 319 arc sec for the GaAs peak and 176 arc sec for the InP peak. The use of Ayers' method¹⁵ to calculate the dislocation density from (004) peak FWHM values, for which the peak broadening is caused by the angular dislocations, underestimates the TDD value compared with ECCI by a factor of two or more, so multiple orders of diffraction angles, such as (115) and (117), are required for accurate dislocation-density estimation. We also note that the TDD value for InP MBL on Si template is higher than that for the same InP MBL on GaAs substrate 12 (i.e., 4.8×10^8 cm $^{-2}$). As far as GaAs/ Si templates, lower TDD values have been reported than the one we found for our GaAs/GaP/Si template. For instance, recently, optimized MOCVD-grown GaAs on (001) Si templates were reported, 16 with a TDD value of $1.4 \times 10^7 \, \text{cm}^{-2}$ and 1.3 nm for RMS surface roughness, although the template thickness was near 3 μ m. An even lower TDD value of $\sim 2 \times 10^6 \, \mathrm{cm}^{-2}$, for a total MBE-grown GaAs thickness of 2.55 μ m, was achieved by using asymmetric step-graded filters 17

The HR-XRD (004) diffraction peaks of the full-QCL structures grown on the InP-on-Si composite template and on InP are shown in Fig. 3 for comparison to the simulated spectrum. The active core of the QCL structure was adopted from Ref. 18, which contains a 35stage In_{0.53}Ga_{0.47}As/Al_{0.52}In_{0.48}As superlattice lattice-matched to InP. Based on the XRD measurement, it was found that the total thickness of the active-core region for the QCL grown on InP may be \sim 2.5% thicker than the target structure, as the superlattice fringe peaks at \sim ±4000 arc sec position shift closer to the InP substrate peak. For the QCL grown on Si, we could not determine the thickness of the activecore region accurately, since the superlattice peaks to the right of the InP peak were hidden by the In_{0.1}Ga_{0.9}As peak. Also, the absence of the zeroth-order superlattice peak near the main InP peak is a good indication that we achieved lattice matching to InP, considering we observed other superlattice fringe peaks. The FWHM of the (004) InP peak is indicative of the overall epitaxial material quality, as it is \sim 144 arc sec for the device on Si and \sim 28 arc sec on InP. This FHWM value obtained from completed laser growth on Si by MOCVD is significantly smaller than that reported for the MBE-grown QCL on Si with a lattice-matched active region, which was 280 arc sec for the InP peak. 10 In addition, distinct satellite peaks are also observed on the compressive side for the QCL on Si, although the peak widths are larger than those on InP. A slight thickness shift of the overall core thickness is observed for QCLs on different substrates compared to

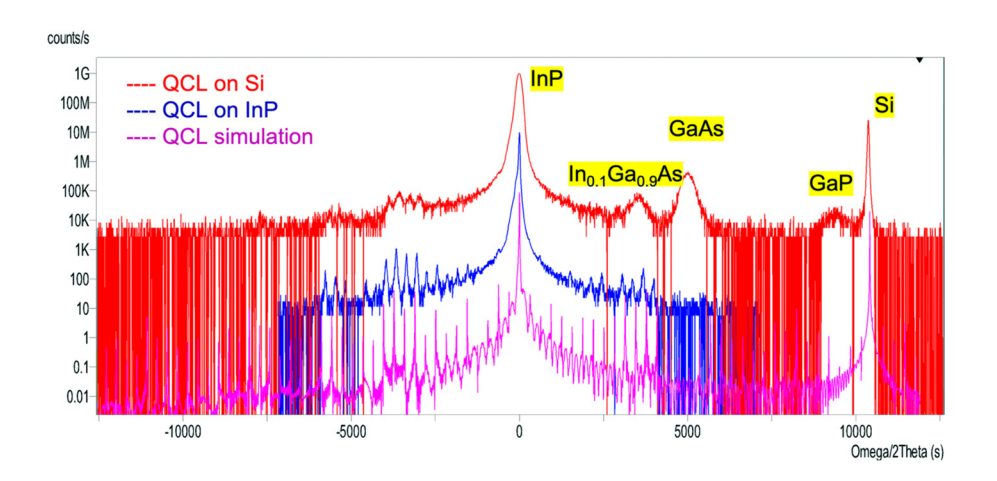


FIG. 3. Comparison of HR-XRD (004) ω – 2θ measurements for the completed laser structure with 35-stage, lattice-matched active-core grown on Si template (red) and on InP (blue) vs the simulated spectrum (pink). The intensity profiles are offset to show the satellite fringe peaks.

the target design, indicating a potential growth rate difference that possibly arises from a surface temperature variation among the substrates. Based on *in situ* reflectance measurements during the QCL growth, a gradual linear intensity reduction was observed during the last few stages of active core growth for the QCL on Si. This reflectance intensity reduction observed during growth might be the result of curvature accumulation across the wafer due to thermal-expansion mismatch. Nevertheless, sharp and well-defined reflection interference fringes could be observed during the entire laser active-core growth for both QCLs, indicating a relatively good surface and interface quality.

Prior to being cleaved into 3 mm-long laser cavities with 25 μ m ridge width, the Si wafer was thinned down to \sim 70 μ m by mechanical lapping. The current was laterally injected with epilayers mounted onto copper heat sinks upwardly, and both facets remained uncoated, similar to that described in Ref. 12. The laser bars were tested at room-temperature under low duty-cycle pulsed operation (200 ns; 20 kHz). As evident from Fig. 4(a), the threshold-current density of devices on Si substrate is \sim 22% lower than that of the devices on InP: 1.50 kA/cm² vs 1.92 kA/cm², which is a similar trend to that reported previously for QCLs grown on lattice-mismatched GaAs substrates. This may reflect a reduced silicon-dopant incorporation within the active-

core superlattice layers due to either preexisting defects or a difference in the surface growth temperature for the Si and InP substrates. In addition, non-uniform growth around the defect sites could potentially reduce the carrier mobility and tunneling efficiency, which would account for the higher series resistance observed for the devices grown on Si. Nevertheless, the peak output power, per facet, delivered from the QCL on Si is higher than the QCL on InP, 1.64 vs 1.47 W. Also, for the QCLs on Si, the single-facet slope efficiency is higher (0.72 vs 0.65 W/A), and the single-facet maximum wall-plug efficiency is higher (2.85 vs 2.50%) than for the QCL on InP. The spectral measurement was performed using a Fourier-transform infrared spectroscopy (FTIR) with high resolution (0.125 cm⁻¹) and shows multi-mode emission wavelengths for both QCLs on Si and InP, in large part due to the wide ridge width (\sim 25 μ m). The center spectral emission for the QCL on Si is slightly longer than for the QCL on InP, centered around \sim 8.1 vs \sim 8.0 μ m at threshold, respectively [Figs. 4(b) and 4(c)]. Both spectral peaks are slightly below the $8.2 \,\mu m$ expected from the target design.¹⁷ One possible reason for this fact could be different local growth rates resulting in quantum-well and barrier thickness variations, as evident from the XRD measurements. The temperature dependence for threshold current and slope efficiency was measured

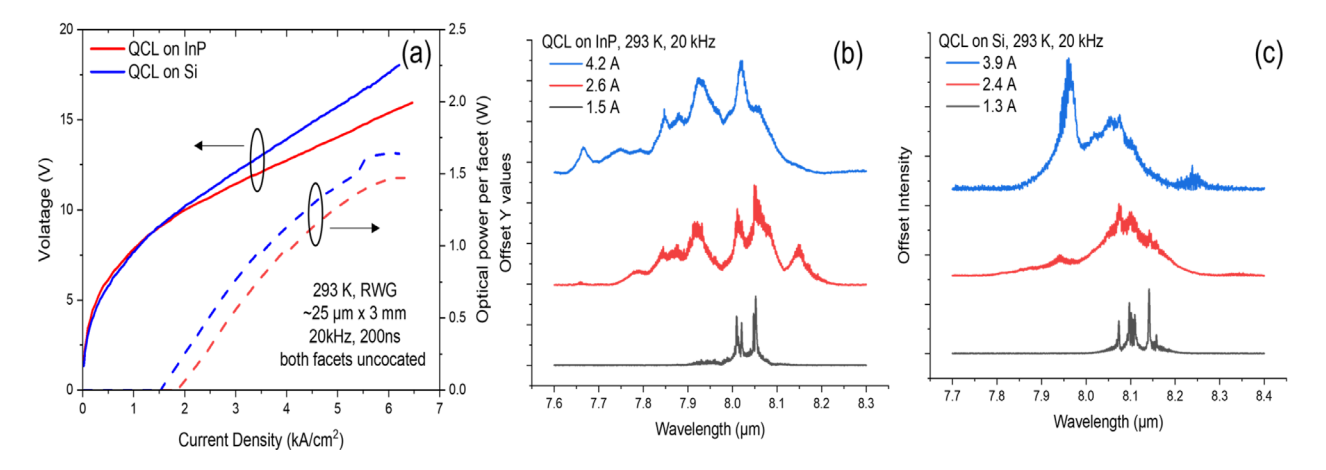


FIG. 4. (a) Characteristics of light power and applied voltage vs current density for \sim 25 μ m-wide and 3 mm-long uncoated ridge-guide devices on InP and on Si, at room-temperature under pulsed operation. Emission spectra for 3 mm-long cavity lasers on (b) InP and (c) on Si, at different drive-current levels.

in the range of 293–353 K and fits to exponential functions. The characteristic temperature values for QCLs on Si are 167 (T_0) and 320 K (T_1), while the values for QCL on InP are 163 (T_0) and 214 K (T_1), respectively. The T_0 value is lower, and the T_1 value is higher compared to values measured for the previously demonstrated QCL on GaAs. ¹² The reasons for these differences are unclear.

While the QCL active-core region is nominally the same as that reported in Ref. 12, there are generally run to run variations, including small variations in layer thickness and doping, which inevitably impact device performance. For that reason, we believe it is relevant to compare the QCL-on-Si device performance to that of devices grown simultaneously on InP. The lower threshold-current density observed for the QCL on InP substrate in this work compared to the QCL on GaAs device reported in previous work¹² (i.e., 1.92 vs 2.42 kA/cm²) is believed to reflect a lower doping density in the active-core region for the current growth. Similarly, the lower dynamic range observed compared with the prior study¹² (i.e., the maximum current density, Jmax, decreased to 6.5 from 9.8 kA/cm²), is also consistent with a lower doping density in the active-core region. In addition, based on the slightly thicker active-core region measured from XRD as well as different lasing-emission wavelength obtained in this work vs the work in Ref. 12 (i.e., 8.1 vs 8.5 μ m), the active-core region is slightly different, reflecting the fact that the layer thicknesses may be off target by \sim 2.5%. These facts may well explain the lower Jth value for the QCL on Si in this work vs the Jth value for the QCL on GaAs in Ref. 12, whereas the InP-on-Si template gives rougher surface and higher TDD value. The existence of threshold dislocations, which act like nonradiative recombination centers in the bandgap for electrons/holes, has a strong impact on conventional diode lasers. In contrast, QCLs are unipolar devices, which operate on intersubband transitions within the conduction band and, thus, are not expected to be susceptible to minority carrier recombination. Furthermore, the very short carrier lifetimes (picosecond range) also make QCLs insensitive to parasitic recombination mechanisms. The insensitivity of QCLs to a highdensity value of TDs was also observed previously.⁶ Note that differences in current spreading between the QCL structures on Si and InP, due to the top-contact configuration and differences in the underlying buffer layers, may also play a role in the observed differences in threshold-current densities. Larger studies are required to statistically quantify the observed performance differences.

In conclusion, an $\sim 8 \, \mu \text{m}$ -emitting InGaAs/AlInAs/InP-based quantum cascade laser is demonstrated by the direct MOCVD heteroepitaxy method onto a (001) Si substrate by employing an MBE-prepared GaAs/Si template. Similar device performance is achieved for the QCL on Si compared to its counterpart grown on InP substrate. Above watt-level output power is obtained (1.64 W/facet) with low threshold-current density (1.5 kA/cm²) under pulsed-current operation at room temperature, despite relatively high surface roughness and high threading dislocation density of the underlying buffer layer. The high performance of MOCVD-grown QCL on Si shows the potential for achieving continuous-wave operation and further confirms the intersubband-laser operation's insensitivity to a relatively high residual TDD value.

The work at the University of Wisconsin-Madison was supported by the National Science Foundation (No. NSF ECCS 1806285) and the Navy Phase I SBIR (Contract No. N68936-22-C-

0022). MicroLink Devices, Inc. acknowledges the support of Navy SBIR support (Contract No. N68936-22-C-0022). The work of Y.W. was carried out in part in the Materials Research Laboratory Central Research Facilities, University of Illinois.

AUTHOR DECLARATIONS

Conflict of Interest

The authors have no conflicts to disclose.

Author Contributions

Shining Xu: Conceptualization (equal); Formal analysis (equal); Investigation (equal); Methodology (equal); Writing – original draft (equal). Shuqi Zhang: Data curation (equal); Investigation (equal). Jeremy Kirch: Formal analysis (equal). Huilong Gao: Data curation (equal). Yiteng Wang: Data curation (equal). Minjoo Larry Lee: Project administration (equal); Writing – review & editing (equal). Sudersena Rao Tatavarti: Funding acquisition (equal). Dan Botez: Writing – review & editing (equal). Luke Mawst: Conceptualization (equal); Supervision (equal); Writing – review & editing (equal).

DATA AVAILABILITY

The data that support the findings of this study are available from the corresponding author upon reasonable request.

REFERENCES

- ¹N. Margalit, C. Xiang, S. M. Bowers, A. Bjorlin, R. Blum, and J. E. Bowers, "Perspective on the future of silicon photonics and electronics," Appl. Phys. Lett. 118(22), 220501 (2021).
- ²J. A. Smith, D. Jevtics, B. Guilhabert, M. D. Dawson, and M. J. Strain, "Hybrid integration of chipscale photonic devices using accurate transfer printing methods," Appl. Phys. Rev. 9(4), 041317 (2022).
- ³E. Tournié, L. Monge Bartolome, M. Rio Calvo, Z. Loghmari, D. A. Díaz-Thomas, R. Teissier, A. N. Baranov, L. Cerutti, and J.-B. Rodriguez, "Midinfrared III–V semiconductor lasers epitaxially grown on Si substrates," Light: Sci. Appl. 11(1), 165 (2022).
- ⁴D. Botez, J. D. Kirch, C. Boyle, K. M. Oresick, C. Sigler, H. Kim, B. B. Knipfer, J. H. Ryu, D. Lindberg, T. Earles, L. J. Mawst, and Y. V. Flores, "High-efficiency, high-power mid-infrared quantum cascade lasers [Invited]," Opt. Mater. Express 8(5), 1378 (2018).
- ⁵Z. Loghmari, J.-B. Rodriguez, A. N. Baranov, M. Rio-Calvo, L. Cerutti, A. Meguekam, M. Bahriz, R. Teissier, and E. Tournié, "InAs-based quantum cascade lasers grown on on-axis (001) silicon substrate," APL Photonics 5(4), 041302 (2020).
- ⁶H. Nguyen-Van, A. N. Baranov, Z. Loghmari, L. Cerutti, J.-B. Rodriguez, J. Tournet, G. Narcy, G. Boissier, G. Patriarche, M. Bahriz, E. Tournié, and R. Teissier, "Quantum cascade lasers grown on silicon," Sci. Rep. 8(1), 7206 (2018).
- ⁷K. Kinjalk, A. Gilbert, A. Remis, Z. Loghmari, L. Cerutti, G. Patriarche, M. Bahriz, R. Teissier, A. N. Baranov, J. B. Rodriguez, and E. Tournié, "Quantum cascade lasers monolithically integrated on germanium," Opt. Express 30(25), 45259 (2022).
- ⁸R. Go, H. Krysiak, M. Fetters, P. Figueiredo, M. Suttinger, X. M. Fang, A. Eisenbach, J. M. Fastenau, D. Lubyshev, A. W. K. Liu, N. G. Huy, A. O. Morgan, S. A. Edwards, M. J. Furlong, and A. Lyakh, "InP-based quantum cascade lasers monolithically integrated onto silicon," Opt. Express 26(17), 22389 (2018).
- ⁹S. Slivken, N. Shrestha, and M. Razeghi, "High power mid-infrared quantum cascade lasers grown on Si," Photonics 9(9), 626 (2022).
- ¹⁰S. Slivken and M. Razeghi, "High power, room temperature InP-based quantum cascade laser grown on Si," IEEE J. Quantum Electron. 58(6), 1–6 (2022).

- ¹¹E. Cristobal, M. Fetters, A. W. K. Liu, J. M. Fastenau, A. Azim, L. Milbocker, and A. Lyakh, "High peak power quantum cascade lasers monolithically integrated onto silicon with high yield and good near-term reliability," Appl. Phys. Lett. 122(14), 141108 (2023).
- ¹²S. Xu, S. Zhang, J. D. Kirch, S. Suri, N. Pokharel, H. Gao, H. Kim, P. Dhingra, M. L. Lee, D. Botez, and L. J. Mawst, "~8.5 μm-emitting InP-based quantum cascade lasers grown on GaAs by metal-organic chemical vapor deposition," Appl. Phys. Lett. 121(17), 171103 (2022).
- ¹³A. Rajeev, B. Shi, Q. Li, J. D. Kirch, M. Cheng, A. Tan, H. Kim, K. Oresick, C. Sigler, K. M. Lau, T. F. Kuech, and L. J. Mawst, "III-V superlattices on InP/Si metamorphic buffer layers for $\lambda \approx 4.8~\mu m$ quantum cascade lasers," Phys. Status Solidi A 216, 1800493 (2018).
- ¹⁴I. Németh, B. Kunert, W. Stolz, and K. Volz, "Heteroepitaxy of GaP on Si: Correlation of morphology, anti-phase-domain structure and MOVPE growth conditions," J. Cryst. Growth 310(7–9), 1595–1601 (2008).

- ¹⁵J. E. Ayers, "The measurement of threading dislocation densities in semiconductor crystals by X-ray diffraction," J. Cryst. Growth 135(1–2), 71–77 (1994).
- 16J. Huang, Q. Lin, W. Luo, L. Lin, and K. M. Lau, "GaAs on (001) Si templates for near-infrared InP quantum dot lasers," J. Appl. Phys. 132(19), 193103 (2022).
- ¹⁷C. Shang, J. Selvidge, E. Hughes, J. C. Norman, A. A. Taylor, A. C. Gossard, K. Mukherjee, and J. E. Bowers, "A pathway to thin GaAs virtual substrate on on-axis Si (001) with ultralow threading dislocation density," Phys. Status Solidi A 218(3), 2000402 (2021).
- ¹⁸Z. Liu, D. Wasserman, S. S. Howard, A. J. Hoffman, C. F. Gmachl, X. Wang, T. Tanbun-Ek, L. Cheng, and F.-S. Choa, "Room-temperature continuous-wave quantum cascade lasers grown by MOCVD without lateral regrowth," IEEE Photonics Technol. Lett. 18(12), 1347–1349 (2006).